Spiking Flip-Flop Memory in Resonant Tunneling Diode Neurons

Giovanni Donati,[1] Dafydd Owen-Newns,[1] Joshua Robertson,[1] Ekaterina Malysheva,[2] Andrew Adair,[1] Jose Figueiredo,[3] Bruno Romeira,[4] Victor Dolores-Calzadilla,[2] and Antonio Hurtado[1]
[1]*Institute of Photonics, SUPA Dept of Physics, University of Strathclyde, Glasgow, United Kingdom*
[2]*Eindhoven Hendrik Casimir Institute, Eindhoven University of Technology, 5600 MB Eindhoven, The Netherlands*
[3]*Centra-Ciências and Departamento de Física, Faculdade de Ciências, Universidade de Lisboa, Lisboa, Portugal*
[4]*International Iberian Nanotechnology Laboratory, Ultrafast Bio- and Nanophotonics Group, Braga, Portugal*

(Received 22 May 2024; accepted 18 November 2024; published 24 December 2024)

We report a spiking flip-flop memory mechanism that allows controllably switching between neural-like excitable spike-firing and quiescent dynamics in a resonant tunneling diode (RTD) neuron under low-amplitude (< 150 mV pulses) and high-speed (ns rate) inputs pulses. We also show that the timing of the set-reset input pulses is critical to elicit switching responses between spiking and quiescent regimes in the system. The demonstrated flip-flop spiking memory, in which spiking regimes can be controllably excited, stored, and inhibited in RTD neurons via specific low-amplitude, high-speed signals (delivered at proper time instants) offers high promise for RTD-based spiking neural networks, with the potential to be extended further to optoelectronic implementations where RTD neurons and RTD memory elements are deployed alongside for fast and efficient photonic-electronic neuromorphic computing and artificial intelligence hardware.

DOI: 10.1103/PhysRevLett.133.267301

Resonant tunneling diodes (RTD) are semiconductor devices designed to benefit from the wave nature of electrons. They are composed of a double barrier quantum well yielding them with inherent electron quantum tunneling effects that result in the occurrence of negative differential resistance (NDR) regions in their current-voltage (I-V) characteristic [1]. By harnessing the highly nonlinear I-V curve of RTDs, a wide range of behaviors, including spiking, multipulse bursting, and oscillatory responses and chaos [2–4], can be elicited, both when operated in isolation or when coupled with external optoelectronic elements [5–9]. RTDs are also capable of achieving ultrahigh (THz range) bandwidth [10], rendering them as promising devices for uses in communications [11]. Exemplar optoelectronic applications of RTD systems include their use as RTD-based electroabsorption modulators working at 900 nm [12] and 1550 nm [13], RTD photodetectors [14], RTD laser diode coupled systems [15], oscillators up to 1.92 THz for wireless communications [11,16], or flip-flop integrated circuit elements switching between two stable voltage values [17]. Interestingly, neuronlike properties may emerge in RTDs when biased in close proximity or within the NDR region, therefore widening their potential applications even to the fields of neuromorphic (brainlike) sensing and computing [18]. Remarkable properties include, for example, excitability (all-or-nothing spike-firing responses) [2,6], and self-feedback regenerative memory operation [19]. These have led to early reports proposing the use of RTDs as spiking (opto)electronic neurons able to deterministically fire spikes in response to electrical and also optical inputs [6,7], and the demonstration of additional neuromorphic properties in RTDs, such as threshold-and-fire responses and refractoriness [6–9]. Nevertheless, while these studies have focused on investigating the triggering of neural-like spiking in RTDs, their potential for yielding key spiking memory responses, crucial for the development of future neuromorphic optoelectronic computing hardware, remains unexplored. This Letter focuses on this key aspect, investigating the temporal dynamical operation of a microscale RTD and demonstrating its ability to deliver long-lasting spiking memory effects. Specifically, this work capitalizes on the bistable regimes [20] that can emerge within the NDR region of the RTD to demonstrate a spiking flip-flop memory. The latter can be switched controllably between neuronlike excitable spiking and quiescent stable dynamics via well-calibrated low-amplitude and high-speed "set" and "reset" input pulses injected into the RTD. By capitalizing on the bistability region within the NDR, not only are we able to demonstrate the spiking memory element of this work, but we can also implement it with a single RTD. This is in stark contrast with previous reports on (nonspiking) RTD flip-flop memory elements (switching between

distinct amplitude states) that required more complex architectures of multiple coupled RTDs for their development [17]. Moreover, we unveil how the spiking nature of the flip-flop memory of this work provides the system an additional temporal processing capability, a key aspect to compute information in spiking neural networks. Considering the compatibility of RTDs with metal-organic chemical vapor deposition, which is the standard for indium phosphide photonic integrated circuits [21], scaling these devices can benefit from the compatibility with existing foundries that manufacture optoelectronic components for diverse applications, including optical networks, sensors, and chips for data center interconnections. This flip-flop spiking memory mechanism offers therefore great prospects for future RTD-based neuromorphic computing hardware, adding crucial memory functionalities (lacking at present) to optoelectronic spiking-based processing platforms.

The RTD of this work has a 3 μm radius circular mesa and was fabricated on a layerstack grown by metal-organic vapor phase epitaxy on a semi-insulating indium phosphide substrate, containing a 1.7 nm AlAs/5.7 nm InGaAs/1.7 nm AlAs double barrier quantum well structure surrounded by highly doped n-InGaAs contact layers [7]. The room-temperature I-V characteristic of the RTD is shown in Fig. 1(a). This is measured when the device is subject to both reverse ([−1.8, 0]V) and forward ([0, 1.8]V) bias conditions. Blue and orange lines in Fig. 1(a) indicate the sweeping direction of the bias voltage, growing from −1.8 V up to 1.8 V in 10 mV steps (blue) and vice versa (orange). A typical N-shaped nonlinear I-V curve appears for both the reverse and forward bias regimes, with peak points appearing respectively at $V_{\text{bias}} = -0.93$ V (reverse bias) and $V_{\text{bias}} = 0.88$ V (forward bias). These two peak points mark the start of both NDR regions followed by valley points in the I-V curve. Crucially, for both NDR regions the RTD exhibits hysteresis cycles (with ≈ 40 mV width) indicating bistable behavior operation. These can be seen in the two insets in Fig. 1(a). To measure the temporal dynamical evolution of this observed bistable behavior in the system at its fast timescales, the output of the RTD is directed to a real-time oscilloscope. Figure 1(b) collects the different dynamical responses exhibited by the RTD when the device is biased with four voltage values and operated in both reverse and forward bias configurations. The voltage values set for the measurements in Fig. 1(b) are highlighted in the I-V curve in Fig. 1(a) with colored dots. Initially, the measured dynamical regimes at the output of the RTD are quiescent for bias voltages below the peak point (black dots). Then, a dynamical transition between quiescent and spiking dynamics occurs when the set bias voltage overcomes the peak points in the I-V curve and enters the NDR region (green dots). The spiking dynamical response persists within the bistable region (red dots) until the valley region is reached (purple dots), where a quiescent response is observed again. If in this situation the bias voltage applied to the RTD is now decreased, bistability is observed, with the system remaining in a quiescent state until the set bias voltage has crossed the bistable region (red dots) in its entirety. Within the hysteresis cycle in the forward and reverse bias regions, the system therefore exhibits spiking or quiescent dynamics depending on which direction the bistable region is entered.

This key observation permits the realization of a flip-flop spiking memory mechanism. To achieve this, the applied bias voltage to the RTD is kept constant at a value within the bistable region (in the forward or reverse bias range) and then fast, set, and reset input voltage pulses are used to escape the bistable region, thus controllably switching the output of the RTD between quiescent and spiking dynamics. We experimentally validate this idea by injecting into the RTD an input signal combining the applied dc bias voltage and an rf input signal. The latter is generated using

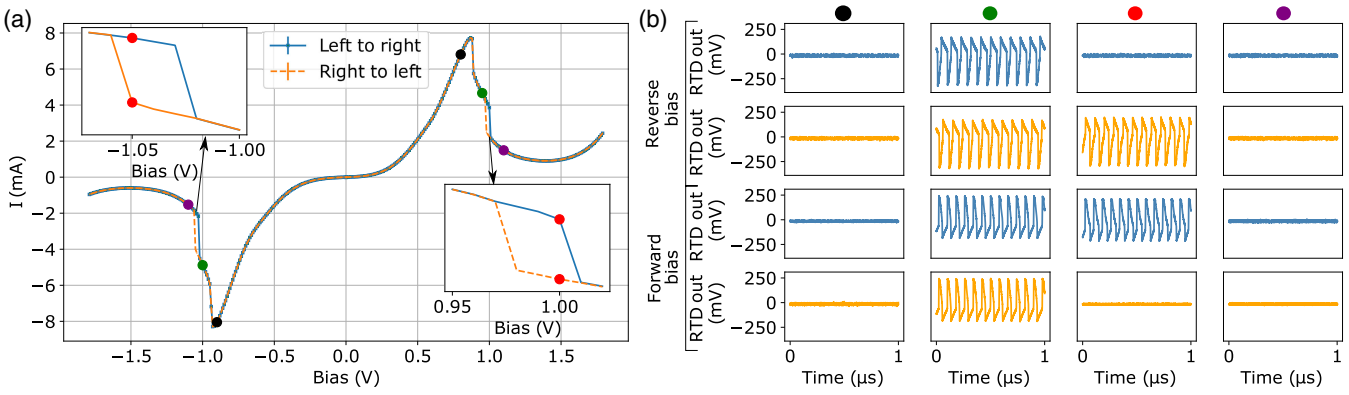

FIG. 1. (a) Average RTD I-V characteristic over three measure repetitions. The two insets highlight the bistable behaviors that our device exhibits within the negative differential resistance regions in both reverse and forward bias conditions. (b) Radio frequency (rf) electrical time response of the RTD at specific forward and reverse bias conditions indicated by colored circles: black, prepeak dynamic; green, postpeak dynamic; red, dynamics within the bistability region; purple, dynamic in the valley region.

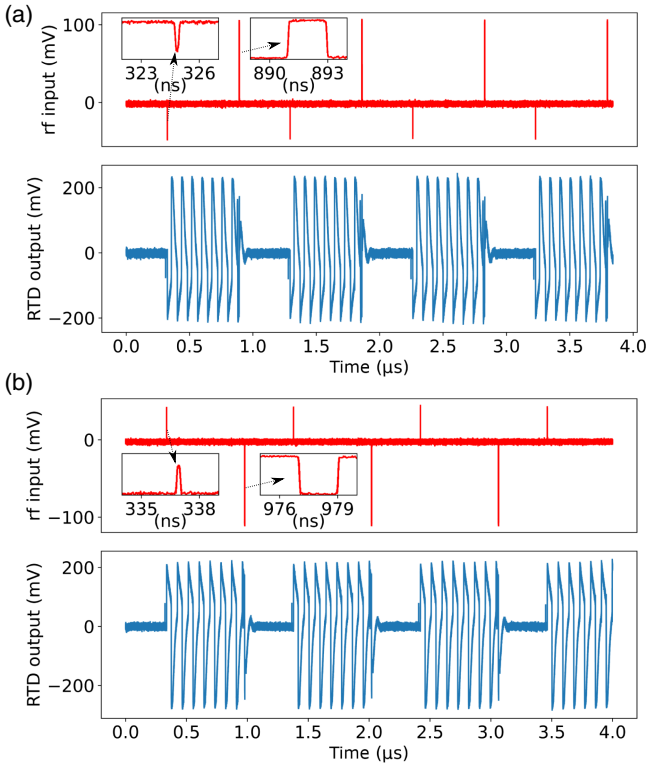

FIG. 2. Flip-flop switching mechanism between spiking and quiescent states using single pulse perturbations. The RTD is biased at (a) $V_b = 1.004$ V (forward bias), and (b) $V_b = -1.057$ V (reverse bias). The set pulses have 47 mV amplitude and 0.2 ns duration, while the reset input pulses have 106 mV amplitude and 2 ns duration.

an arbitrary waveform generator (see setup scheme in Appendix A) and consists of a series of set and reset input voltage pulses, separated by a set delay time. Figures 2(a) and 2(b) show two examples of the dynamical spiking flip-flop memory mechanism when the RTD is operated in forward [Fig. 2(a)] and reverse [Fig. 2(b)] bias, respectively. In the forward bias case [Fig. 2(a)], the system is first set to operate in a quiescent dynamical state, by tuning the bias voltage from 0 to 1.2 V and then decreasing the voltage to the set value $V_{\text{bias}} = 1.004$ V, within the bistable region. In that situation, the rf input signal [red time trace in the top plot of Fig. 2(a)] is injected into the RTD to activate the spiking flip-flop memory mechanism. The arrival of set input pulses switch the RTD output response from the initial quiescent to a spiking dynamical regime, which persists even after the set pulses are over. In this first case of analysis, the set pulses are configured with negative polarity. Therefore, the arrival of the set pulse temporally reduces the total voltage applied to the RTD to a value below the hysteresis cycle and to the region of the I-V curve in which a spiking response is obtained [see Fig. 1(b)]. When the set pulse ends, the total input voltage recovers back to the initial bias value within the bistable region, but now entering into it with the voltage direction that preserves the spiking dynamical output [Fig. 1(a), blue line]. The newly set spiking dynamical response from the RTD is then controllably switched back to the original quiescent state by introducing after a certain delay time a reset input voltage pulse. The latter has positive polarity to ensure that the system temporally exits and reenters the bistable region in the voltage direction that preserves the quiescent state, as shown in Fig. 2(a) (blue time trace). The same spiking memory methodology also applies when the RTD neuron is operated in reverse bias, $V_{\text{bias}} = -1.057$ V [see in Fig. 2(b)]. There are only two observable differences between the results in Figs. 2(a) and 2(b). The first one is that in the reverse bias case, the set and reset pulses switching controllably between quiescent and spiking dynamical regimes are configured now with positive and negative polarity, respectively, see red time trace in Fig. 2(b)]. Set and reset pulse amplitudes are therefore swept according to the operated (forward and reverse) bias configuration. The second difference is that the spiking regimes are obtained now with reverse polarity, illustrating the versatility of the system, permitting operation with negative and positive input pulses and delivering spikes of different polarities and hence enabling enhanced neuromorphic computational capabilities. Importantly, the results presented are obtained using high-speed and low-energy input signals. Specifically, the set pulses are configured with a temporal duration of only 200 ps and 47 mV amplitude, while the reset pulses are configured with a duration of 2 ns and 106 mV in amplitude.

Remarkably, we find that in addition to their amplitude, the time at which the reset pulses are delivered to the RTD plays a major role in the achievement (or not) of the switching mechanism. This time dependence adds an extra degree of freedom in the computational properties of this RTD spiking memory system when compared to traditional electronic [22] and optical [23] flip-flop memory components switching between two distinct (nonspiking) stable states. To illustrate this behavior, in Fig. 3(a) we studied the response of the system to a multiplicity of delay times between set and reset pulses. Here, the RTD is set to deliver initially a spiking dynamical response triggered by a first input set pulse (with positive or negative polarity, depending on the bias configuration selected). In this situation, reset pulses are delivered at different delay times (with respect to the set pulse). In each case of analysis we collected the response of the RTD during the 400 ns following the arrival of the reset pulse, and calculated the difference between maximum and minimum amplitude in that time frame. The resulting values, plotted against the delay between set and reset pulses in Fig. 3(a), will be therefore large or small when the system is in a spiking and quiescent state, respectively, given the different amplitude excursions between the continuous spiking events and the constant quiescence levels that follow the reset pulse. The study is performed for both the reverse [Fig. 3(a), blue line]

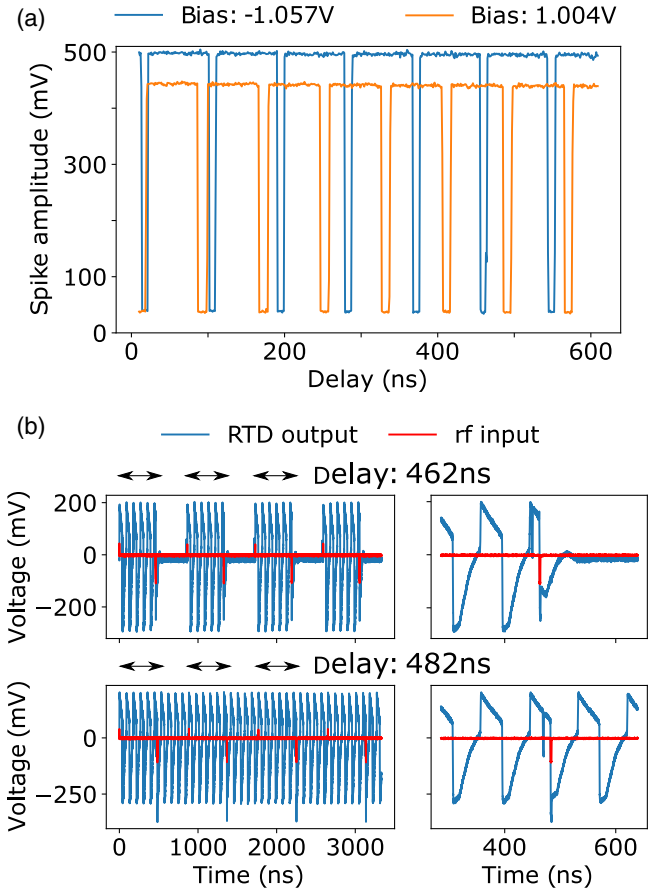

FIG. 3. (a) RTD spiking amplitude after the injection of a reset input pulse, as a function of the delay time, for both reverse (bias −1.057 V) and forward (bias 1.004 V) configurations. (b) rf input and RTD response for two specific reset pulse delay times in reverse bias configuration: 462 ns (above) and 482 ns. An enlargement on the right column highlights the stage of the dynamics when the reset pulse arrives. Note that the RTD response seems to drop even before the arrival of the input pulse, but this is an artifact due to a replica of the arbitrary waveform generator (AWG) signal that, through the splitter shown in Fig. 4 (see Appendix A), is also acquired (in advance) from the oscilloscope.

and forward [Fig. 3(a), orange line] bias scenarios, and with the delay time in the range [10–610] ns with 1 ns resolution. Figure 3(a) clearly shows an emerging binary pattern whereby this amplitude curve oscillates between a minimum value, corresponding to the cases in which the reset pulse is able to suppress the spiking dynamical regime switching back the output state to quiescence, and a maximum level in which the arrival of the reset pulse is unable to switch the system to quiescence and the spiking dynamical output persists. Figure 3(a) therefore highlights the achievement of an all-or-nothing temporal switching response depending on the delay time between set and reset pulse considered. In particular, the spike amplitude value associated to each delay time in Fig. 3(a) is the largest one (following the reset pulse) found across 200 switching acquisitions. Therefore, the dips appearing in the curves in Fig. 3(a) indicate that for those delay times the reset pulse suppresses the spiking activity over all the 200 acquisitions, thus reflecting the reliability of the proposed spiking flip-flop memory. Moreover, Fig. 3(a) describes a clear periodic dependence of the reset-pulse switching mechanism in the spiking flip-flop memory as a function of the delay time between set and reset pulses. To grasp the origin of this dependency, we report in Fig. 3(b) two examples of temporal responses in the RTD achieved for two delay times of 462 and 482 ns, respectively. For the results in Fig. 3(b) the RTD was reverse-biased with a voltage of −1.057 V [see blue curve in Fig. 3(a)]. Figure 3(b) reveals that for a case in which the switching from the spiking to quiescent state is effective (in this case a delay of 462 ns was set), the reset negative pulse (see red curve) competes against the positive phase of the spike emitted by the RTD [see enlargement in the top row in Fig. 3(b)] suppressing it and switching the system to a constant output. This consideration allows one to relate the dip widths in Fig. 3(a) with the slow phase of the evolution of an RTD spike toward its peak biasing point [4]. This feature permits one to tune the width of the temporal regions where the switching transition back to quiescence is completed [dips in Fig. 3(a)] by controlling the applied voltage bias within the bistable region. On the other hand, for a case in which the switching from spiking to quiescence is not completed (delay of 482 ns), the reset negative pulse is almost coherent with the spiking dynamics [see enlargement in the bottom row of Fig. 3(b)], therefore supporting it and not contributing to its suppression. This situation is kept also for larger delay times in which the negative reset pulse arrives coinciding with the negative phase of the spike fired by the RTD, further supporting it and not contributing to its suppression. This behavior is maintained until a larger delay time for which the negative reset pulse arrives coinciding with the positive excursion of the next spike fired by the RTD, and is able to suppress it once again. Since the RTD fires spikes with a periodicity of ≈90 ns, given by the device's refractory period [7], this explains the periodicity of the time dependency observed in Fig. 3(a). This behavior also explains why larger amplitudes are required for the reset (106 mV) than for the set (47 mV) pulses to achieve the spiking flip-flop memory effects. On one hand, the amplitude of the set pulse is related to the width of the bistable region (≈40 mV), which needs to be overcome to bring the system into the spiking dynamical region in the device's I-V characteristic. On the other hand, the reset pulse needs to outcompete the large amplitude excursion of a spike in order to suppress it. For example, reset pulses with lower amplitudes, even when delivered at the correct delay values in Fig. 4(a), were not sufficiently strong and the switching mechanism could not be fully completed. The system performance was tested against perturbations arising from the arrival of multiple

consecutive set (or reset) pulses at unintended times. The system demonstrated robustness and showed negligible effects when perturbed by secondary set and reset pulses. Additionally, the RTD spiking dynamical responses remained stable even when subjected to high-amplitude set pulses, with values tested up to 222 mV. We must note that the amplitude of the set pulse had a minor effect on the exact timing at which the first spike event was elicited, with stronger set pulses yielding a slightly faster spiking response (by around 1 ns for the RTD neuron of this work). This would in turn modify accordingly the exact timing of the spikes subsequently fired by the RTD, thus allowing one to shift controllably, albeit by a small margin, the delay pattern in Fig. 3(a). Note that in these experiments, longer reset pulses (2 ns) than set pulses (200 ps) were used with the only purpose of sampling their delivery time during the oscilloscope acquisition (having a sampling period of 2.5 ns). Nevertheless, it was checked that when reset pulses have an equal duration to the set pulses (200 ps) and are delivered at the proper time indicated in Fig. 3(a), the spiking flip-flop memory still operated successfully, but at the cost of a larger reset pulse amplitude (187 mV). Finally, the potential of the system to operate with optical input signals was also tested (see Appendix B), and certified over timescales (tens of seconds) much longer than the duration of the individual spike ($\approx 10^{-7}$ s).

In summary, this Letter demonstrates a fast and efficient RTD spiking flip-flop memory that can be controllably switched between continuous spiking and quiescent dynamics via fast (ns rate) and low-amplitude set and reset pulses (< 150 mV amplitude), while biasing the RTD within a bistable region in the NDR. Versatile operation is demonstrated, as the spiking flip-flop memory effects can be achieved with the RTD operated in reverse and forward bias regimes, with inputs and spiking outputs of different polarities and in fully electronic and optoelectronic configurations (see Appendix B). The transition from spiking to quiescent dynamics strongly depends on the delay time with which the reset pulse is delivered to the RTD, thus yielding the system with an additional temporal processing capability, a key aspect in spiking neural networks to compute information. In this regard, such flip-flop memory function opens their use for application in network regions where the timing of the input information is meaningful. Therefore, rather than in networks or systems adopting rate coding techniques and frequent spike-firing process, RTDs with memory functionalities may be involved in networks or systems dealing with sparse input information. For example, they can be envisioned as neurons in the input layer of a network merging different sensory input information, with their state switching only for specific delay patterns between two different stimuli. In this way this delayed detection is stored and transmitted in the form of spikes (or not) to follow up layers. If a forced reset is needed, for example for specific system clocks, the switching timing property can be bypassed by delivering to the RTD an appropriate reset pulse with a much longer duration than the RTD spike duration (see Appendix B). We also proved the reliability of the proposed configuration over extended timescales (up to tens of seconds, see Appendix B) much longer than the spiking refractory period (tens of ns), and performed theoretical analyses validating the experimental findings at faster sub-ns timescales (see Supplemental Material [24]). Simulation results reveal that RTD circuit inductance, capacitance, and resistance are key for targeting the desired spiking regime, with the inductance and capacitance influencing also the width of the bistable region [4]. Under this view, future design engineering that allow an adjustable control of these RTD circuits can provide physical trainable parameters that tailor the flip-flop switching mechanism in RTD-based neurons *ad hoc* for the specific task at hand. The above attributes, when RTDs are coupled or equip optoelectronic integrated components (e.g., photodetectors [14], light sources [7,15], and optical waveguides [12,13]), are promising for the realization of integrated photonic-electronic spiking networks for use in future high-speed and energy-efficient neuromorphic computing technologies. Furthermore, the identified conceptual elements underpinning the RTD spiking flip-flop memory of this work, namely excitability, spiking dynamical regimes, bistability, and time-dependent spiking and switching responses, pave the way toward future demonstrations of spiking flip-flop memory elements in other systems also exhibiting bistable transitions between spiking and quiescent states (e.g., silicon microring resonators [25]), as well as to other electronic neurons [26,27].

Acknowledgments—The authors acknowledge support from the UKRI Turing AI Acceleration Fellowships Programme (EP/V025198/1), from the EU Pathfinder Open project "SpikePro," from the Fraunhofer Centre for Applied Photonics, FCAP, and from the Fundação para a Ciência e a Tecnologia (FCT) project 2022.03392.PTDC–META-LED.

Data availability—The data that support the findings of this article are openly available at [28].

[1] C. Ironside, B. Romeira, and J. Figueiredo, *Resonant Tunnelling Diode Photonics Devices and Applications* (IOP Publishing, Bristol, 2023).

[2] B. Romeira, J. Javaloyes, C. N. Ironside, J. M. Figueiredo, S. Balle, and O. Piro, Excitability and optical pulse generation in semiconductor lasers driven by resonant tunneling diode photo-detectors, Opt. Express **21**, 20931 (2013).

[3] B. Romeira, R. Avó, J. Javaloyes, S. Balle, C. N. Ironside, and J. M. Figueiredo, Stochastic induced dynamics in neuromorphic optoelectronic oscillators, Opt. Quantum Electron. **46**, 1391 (2014).

[4] I. Ortega-Piwonka, O. Piro, J. Figueiredo, B. Romeira, and J. Javaloyes, Bursting and excitability in neuromorphic resonant tunneling diodes, Phys. Rev. Appl. **15**, 034017 (2021).
[5] I. Ortega-Piwonka, M. Hejda, J. Alanis, J. Lourenço, A. Hurtado, J. Figueiredo, B. Romeira, and J. Javaloyes, Spike propagation in a nanolaser-based optoelectronic neuron, Opt. Mater. Express **12**, 2679 (2022).
[6] M. Hejda, J. A. Alanis, I. Ortega-Piwonka, J. Lourenço, J. Figueiredo, J. Javaloyes, B. Romeira, and A. Hurtado, Resonant tunneling diode nano-optoelectronic excitable nodes for neuromorphic spike-based information processing, Phys. Rev. Appl. **17**, 024072 (2022).
[7] M. Hejda, E. Malysheva, D. Owen-Newns, Q. R. Ali Al-Taai, W. Zhang, I. Ortega-Piwonka, J. Javaloyes, E. Wasige, V. Dolores-Calzadilla, J. M. Figueiredo *et al.*, Artificial optoelectronic spiking neuron based on a resonant tunnelling diode coupled to a vertical cavity surface emitting laser, Nanophotonics **12**, 857 (2023).
[8] W. Zhang, M. Hejda, E. Malysheva, Q. R. A. Al-Taai, J. Javaloyes, E. Wasige, J. M. Figueiredo, V. Dolores-Calzadilla, B. Romeira, and A. Hurtado, Tunable presynaptic weighting in optoelectronic spiking neurons built with laser-coupled resonant tunneling diodes, J. Phys. D **56**, 084001 (2023).
[9] Q. R. A. Al-Taai, M. Hejda, W. Zhang, B. Romeira, J. M. Figueiredo, E. Wasige, and A. Hurtado, Optically-triggered deterministic spiking regimes in nanostructure resonant tunnelling diode-photodetectors, Neuromorph. Comput. Eng. **3**, 034012 (2023).
[10] Y. Nishida, N. Nishigami, S. Diebold, J. Kim, M. Fujita, and T. Nagatsuma, Terahertz coherent receiver using a single resonant tunnelling diode, Sci. Rep. **9**, 18125 (2019).
[11] D. Cimbri, J. Wang, A. Al-Khalidi, and E. Wasige, Resonant tunneling diodes high-speed terahertz wireless communications-a review, IEEE Trans. Terahertz Sci. Technol. **12**, 226 (2022).
[12] J. Figueiredo, C. Stanley, A. Boyd, C. Ironside, S. McMeekin, and A. Leite, Optical modulation in a resonant tunneling relaxation oscillator, Appl. Phys. Lett. **74**, 1197 (1999).
[13] J. L. Figueiredo, C. N. Ironside, and C. R. Stanley, Electric field switching in a resonant tunneling diode electroabsorption modulator, IEEE J. Quantum Electron. **37**, 1547 (2001).
[14] B. Romeira, L. M. Pessoa, H. M. Salgado, C. N. Ironside, and J. M. Figueiredo, Photo-detectors integrated with resonant tunneling diodes, Sensors **13**, 9464 (2013).
[15] T. J. Slight and C. N. Ironside, Investigation into the integration of a resonant tunnelling diode and an optical communications laser: Model and experiment, IEEE J. Quantum Electron. **43**, 580 (2007).
[16] T. Maekawa, H. Kanaya, S. Suzuki, and M. Asada, Oscillation up to 1.92 THz in resonant tunneling diode by reduced conduction loss, Appl. Phys. Express **9**, 024101 (2016).
[17] K. Sano, K. Murata, T. Otsuji, T. Akeyoshi, N. Shimizu, and E. Sano, An 80-Gb/s optoelectronic delayed flip-flop IC using resonant tunneling diodes and uni-traveling-carrier photodiode, IEEE J. Solid-State Circuits **36**, 281 (2001).
[18] B. Romeira, R. R. Adão, J. B. Nieder, Q. Al-Taai, W. Zhang, R. H. Hadfield, E. Wasige, M. Hejda, A. Hurtado, E. Malysheva *et al.*, Brain-inspired nanophotonic spike computing: Challenges and prospects, Neuromorph. Comput. Eng. **3**, 033001 (2023).
[19] B. Romeira, J. M. Figueiredo, and J. Javaloyes, Delay dynamics of neuromorphic optoelectronic nanoscale resonators: Perspectives and applications, Chaos **27**, 114323 (2017).
[20] N. Kluksdahl, A. Kriman, D. Ferry, and C. Ringhofer, Intrinsic bistability in the resonant tunneling diode, Superlattices Microstruct. **5**, 397 (1989).
[21] M. Smit, X. Leijtens, H. Ambrosius, E. Bente, J. Van der Tol, B. Smalbrugge, T. De Vries, E.-J. Geluk, J. Bolk, R. Van Veldhoven *et al.*, An introduction to inp-based generic integration technology, Semicond. Sci. Technol. **29**, 083001 (2014).
[22] J.-M. Portal, M. Bocquet, M. Moreau, H. Aziza, D. Deleruyelle, Y. Zhang, W. Kang, J.-O. Klein, Y.-G. Zhang, C. Chappert *et al.*, An overview of non-volatile flip-flops based on emerging memory technologies, J. Electron. Sci. Technol. **12**, 173 (2014).
[23] T. Alexoudi, G. T. Kanellos, and N. Pleros, Optical ram and integrated optical memories: A survey, Light **9**, 91 (2020).
[24] See Supplemental Material at http://link.aps.org/supplemental/10.1103/PhysRevLett.133.267301 for modeling results of a spiking flip-flop memory in resonant tunneling diode neurons.
[25] S. Biasi, G. Donati, A. Lugnan, M. Mancinelli, E. Staffoli, and L. Pavesi, Photonic neural networks based on integrated silicon microresonators, Intell. Instrum. Comput. **3**, 0067 (2024).
[26] I. Sourikopoulos, S. Hedayat, C. Loyez, F. Danneville, V. Hoel, E. Mercier, and A. Cappy, A 4-fj/spike artificial neuron in 65 nm CMOS technology, Front. Neurosci. **11**, 123 (2017).
[27] J. H. Wijekoon and P. Dudek, Compact silicon neuron circuit with spiking and bursting behaviour, Neural Netw. **21**, 524 (2008).
[28] G. Donati, Data for: "Spiking flip flop memory in Resonant Tunneling Diode Neurons" (2024), 10.15129/85a8aefa-1555-4936-b6e9-0db29b9d8d90.

End Matter

Appendix A: Experimental apparatus enabling fully electronics flip-flop memory functionality—Figure 4 plots the experimental setup used for the characterization of the static and dynamic properties of the RTD spiking memory element. A bias controller (keysight E36312A) is used for both setting the desired bias voltage to the RTD and reading the correspondent output current. An arbitrary waveform generator (AWG, keysight M8190A, 12 GSa/s) allows generating rf waveforms with set and reset voltage pulses. These pulses propagate toward a

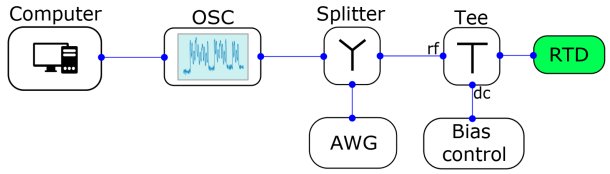

FIG. 4. Sketch of the experimental setup. AWG, arbitrary waveform generator; OSC, oscilloscope; Tee, bias tee.

splitter and then a bias tee ([0.01–12.4] GHz bandwidth range), where they are combined with the bias dc signal. The temporal dynamical evolution in the system at its fast (spiking) timescales is measured by directing the rf component of the RTD output to a high-speed real-time oscilloscope (OSC, Rohde & Schwarz, 16 GHz bandwidth), which is then connected to a computer for data storing.

Appendix B: Optoelectronic experimental configuration enabling flip-flop memory functionality—The experimental setup used to investigate the operation of an optically activated RTD flip-flop spiking memory is shown in Fig. 5(a). This has been updated to include an input optical line generated with a tunable laser source (TLS, Santec WSL-110) emitting a continuous wave optical signal at the set wavelength of 1546 nm. The continuous wave optical signal propagates through a polarization controller (PC) and a variable optical attenuator (VOA) to control the polarization and optical power of the light signal from the TLS, before being amplitude modulated using a Mach-Zehnder (MZ) modulator. The MZ modulator is driven according to a dc bias voltage (setting the MZ operating point at the bottom of its transfer function) and an amplified rf signal provided by the AWG in the setup, to encode input pulses in the optical line. The modulated optical signal, having an average optical power of 9 μW, is equally divided along two lines using a fiber-optic coupler, therefore producing two copies of the input optical information that terminate in two identical fast photodetectors (Thorlabs PDA8GS, 9.5 GHz), respectively. One of the photodetectors, PD2 in Fig. 5(a), serves as a monitor of the optical input power, while the output from PD1, in the other line, is connected to the rf port of the bias tee for its injection into the RTD (Fig. 4). Therefore, the RTD is now subject to both an electrical dc voltage bias and an rf signal input generated optically. The optoelectronic flip-flop spiking memory mechanism is tested in the way illustrated graphically in Fig. 5(b) (left). The RTD neuron is reverse-biased with a voltage of $V_{\text{bias}} = -1.05$ V, with positive (optically generated) set pulses triggering the spiking dynamics in the RTD spiking memory, whereas negative reset pulses are electronically

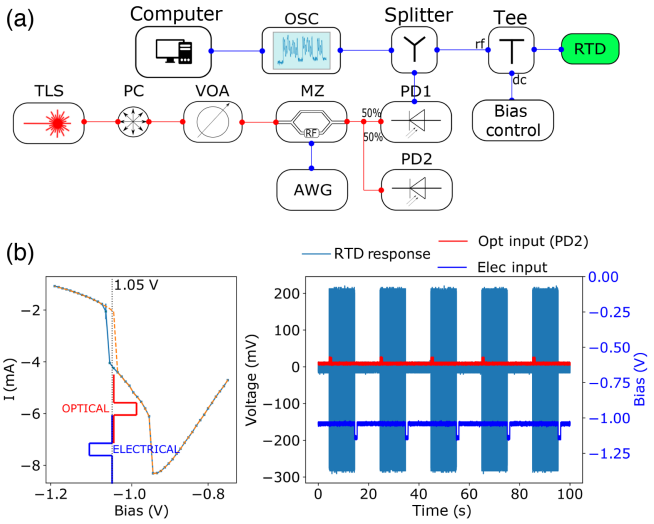

FIG. 5. Electro-optical switching. (a) Upgraded system scheme with both electrical (blue connections) and optical (red connections) lines. (b) RTD response under an electro-optic flip-flop memory over tens of seconds timescale. The RTD spiking dynamics are triggered optically and suppressed electronically.

generated and injected into the device to restore the quiescent state. The reset pulses are now generated by temporally decreasing the bias voltage provided by the power source toward the valley region. These have a longer temporal duration of 1 s to accommodate the bias controller sweeping speed, when moving from the bistable region ($V_{\text{bias}} = -1.05$ V) toward the valley region ($V_{\text{bias}} = -1.15$ V) and vice versa. Similarly, we generated optical perturbations lasting for 1 s, formed by a series of short 1 ns-long optical pulses with 100 ns repetition rate. Between each 1s-long optical perturbation window range, the AWG modulation (driving the MZ modulator) is turned off. Input electrical and optical perturbations are shown in Fig. 5(b) in blue and red color traces, respectively. The RTD's spiking memory response is also shown in Fig. 5(b) (light-blue curve time trace) clearly revealing the induced flip-flop switching between continuous spiking and quiescent dynamical regimes. The measurement results in Fig. 5(b) were purposely taken over a long-lasting temporal range of a total tens of seconds (a timescale much higher than the duration of the individual spike, $\approx 10^{-7}$ s), to confirm the long-term stability and consistency of the spiking flip-flop memory mechanism in the RTD.

The electro-optical switching has been also tested when forward bias the RTD in the bistable region (not shown). In this case, positive bias perturbations (reset pulses) were used to escape the bistable region and restore a quiescent state, while negative electrical pulses, optically generated, were used to initiate the spiking dynamic. Note that to

obtain negative electrical pulses, optically generated, the MZ is biased at the top of its transfer function and then perturbed using positive (or even negative) AWG voltage pulses. The resulting optical pulses emerge in this way as negative perturbations of the higher optical base level. After being detected, they are encoded in negative voltage pulses thanks to the bias tee rf port filtering effects, and then input to the RTD. The latter configuration is therefore disadvantaged concerning the reversed-bias one, as it relies on a higher average input optical power (to generate negative optical pulses the optical base floor must be higher) and filtering effects (to finally achieve negative electrical pulses) given by additional setup instruments than the RTD.